Kinetic or Dynamic Control on a Bifurcating Potential Energy Surface? An Experimental and DFT Study of Gold-Catalyzed Ring Expansion and Spirocyclization of 2-Propargyl-*β*-tetrahydrocarbolines

Lei Zhang,[†,§] Yi Wang,[‡,§] Zhu-Jun Yao,[†] Shaozhong Wang,*,[†] and Zhi-Xiang Yu*,[‡]

[†]State Key Laboratory of Coordination Chemistry, School of Chemistry and Chemical Engineering, Nanjing University, Nanjing 210093, China

[‡]Beijing National Laboratory for Molecular Sciences (BNLMS), Key Laboratory of Bioorganic Chemistry and Molecular Engineering of Ministry of Education, College of Chemistry, Peking University, Beijing 100871, China

S *Supporting Information*

ABSTRACT: In classical transition state theory, a transition state is connected to its reactant(s) and product(s). Recently, chemists found that reaction pathways may bifurcate after a transition state, leading to two or more sets of products. The product distribution for such a reaction containing a bifurcating potential energy surface (bPES) is usually determined by the shape of the bPES and dynamic factors. However, if the bPES leads to two intermediates (other than two products), which then undergo further transformations to give different final products, what factors control the selectivity is still not fully examined. This missing link in transition state theory is founded in the present study. Aiming to develop new methods for the synthesis of azocinoindole derivatives, we found that 2-propargyl-*β*-tetrahydrocarbolines can undergo ring expansion and spirocyclization under gold catalysis. DFT study revealed that the reaction starts with the intramolecular cyclization of the gold-activated 2-propargyl-*β*-tetrahydrocarboline with a bPES. The cyclization intermediates can not only interconvert into each other via a [1,5]-alkenyl shift, but also undergo ring expansion (through fragmentation/protodeauration mechanism) or spirocyclization (through deprotonation/protodeauration mechanism). Detailed analysis of the complex PESs for substrates with different substituents indicated that the reaction selectivity is under dynamic control if the interconversion of the intermediates is slower than the ring expansion and spirocyclization processes. Otherwise, the chemical outcome is under typical kinetic control and determined by the relative preference of ring expansion versus spirocyclization pathways. The present study may enrich chemist's understanding of the determinants for selectivities on bPESs.
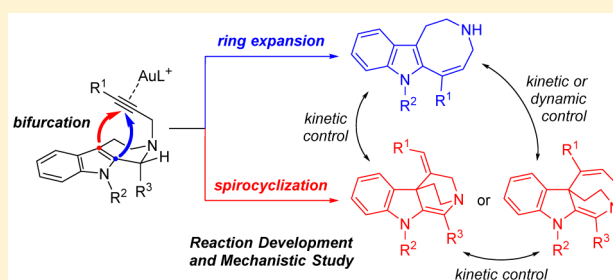
■ INTRODUCTION

Transition state theory has been rooted in the chemical sciences for understanding the kinetics and selectivities of chemical transformations. In traditional transition state theory, a transition state connects one set of reactants with one set of products. Recently, chemists found that one transition state may lead to two (or more) sets of products simultaneously on a bifurcating potential energy surface (bPES).[1−3] As shown in Figure 1A, the reaction first proceeds through transition state **TS1A**. Then the reaction pathways bifurcate at the valley−ridge inflection (VRI) point[1] to give two products **P1A** and **P2A**, which are connected by another transition state **TS2A**. In most cases, the product distribution for the reaction in Figure 1A is controlled by the shape of the PES and the resulting dynamic factors.[1] Usually, theoretical chemists must resort to simulate numerous trajectories utilizing quantum molecular dynamics to estimate the ratio of the final products.[1,2,3i]

Figure 1B−D depicts the situations in which surface bifurcations lead to two intermediates (other than two products),

which then undergo further transformations to give the final products.[4] In the case of Figure 1B, intermediates **IN1B** and **IN2B** cannot interconvert via **TS2B** because the barrier for the interconversion is higher than those for the transformations of **IN1B** (into **P1B**) and **IN2B** (into **P2B**). Therefore, the product distribution is equal to the ratio of **IN1B** and **IN2B**, which is controlled by nonstatistical dynamic factors. In the case of Figure 1C, **IN1C** cannot convert to **IN2C** because the activation energy for the interconversion transition state **TS2C** is higher than that for **TS3C**, which connects **IN1C** and **P1C**. In contrast, conversion from **IN2C** to **IN1C** is kinetically favored over the transformation of **IN2C** into **P2C** because the activation energy for **TS2C** is lower than that for **TS4C**, which connects **IN2C** and **P2C**. Therefore, **P1C** will be formed predominantly according to the traditional transition state theory and the reaction in Figure 1C is under kinetic control. In the case of Figure 1D, **IN1D** and
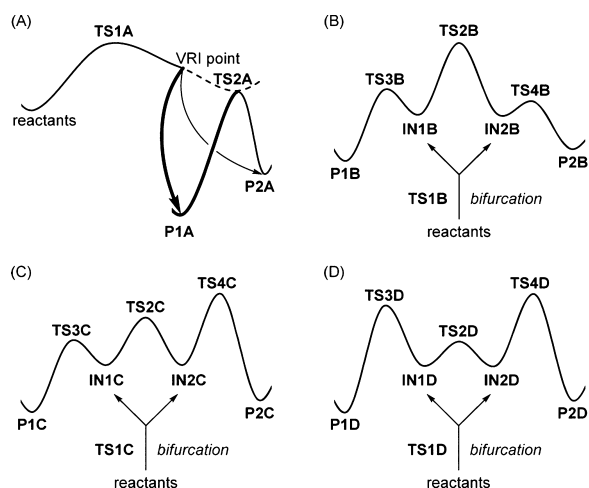
Figure 1. Surface bifurcations in four reaction systems.

IN2D are in rapid equilibrium because the barrier for the interconversion is lower than that for transformation of these two intermediates into the final products. In this case, the Curtin−Hammett principle[5] applies and the reaction is under typical kinetic control (the ratio of **P1D** and **P2D** is determined by the energy difference of **TS3D** and **TS4D**). Reactions involving post-transition-state surface bifurcations are rare. Up to now, only limited numbers of examples have been reported.[1−3] To the best of our knowledge, no reaction system including all the situations discussed in Figure 1B−D has been observed. Finding such a reaction system experimentally and then understanding the reaction selectivity theoretically will greatly enrich chemists' understanding of the determinants for selectivities on bPESs.

Herein, we report our discovery of such a reaction system, the gold-catalyzed transformations[6] of 2-propargyl-β-tetrahydrocarbolines (Scheme 1), involving all cases shown in Figure 1B−D.

Scheme 1. Ring Expansion and Spirocyclization of 2-Propargyl-β-tetrahydrocarbolines
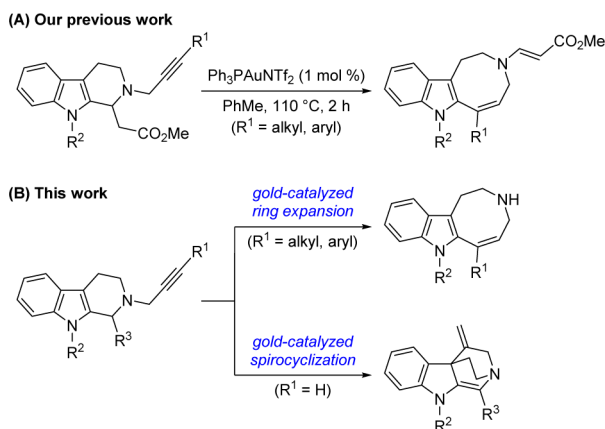
The discovery of such reactions was driven by our desire to develop a general method for the synthesis of the unique tricyclic azocinoindole ring system[7,8] found in natural alkaloids, such as okaramines,[9] grandilodines,[10] lundurines,[11] and lapidilectines.[12] Until now, synthesis of medium-sized heterocycles, including the azocinoindole derivatives, still represents a challenge in today's science of synthesis, considering that the reactions and strategies to construct the medium-sized-ring systems are limited.[13] Previously, we developed a gold-catalyzed ring expansion of 2-

propargyl-β-tetrahydrocarbolines to synthesize functionalized azocinoindoles (Scheme 1A).[14] The 2-propargyl-β-tetrahydrocarboline substrate can be easily prepared in two steps from tryptamine and the scope of the reaction is broad with good yields. However, we found that the methoxycarbonylmethyl group at the C1-position of the β-tetrahydrocarboline is indispensable for the ring expansion, which greatly limited the practicality of such a reaction in synthesis.

After extensive screening of the reaction conditions, we were glad to find that acidic additives are efficient to promote the ring expansion, in which case, unprotected secondary amine products can be obtained in excellent yields (Scheme 1B, top). Furthermore, we found that the terminal R^1 group on the alkyne moiety plays a crucial role in determining the outcome of the reaction. For terminal alkyne substrate, dearomatizing spirocyclization[15] product is observed as the major product instead of the desired azocinoindole (Scheme 1B, bottom).

Meanwhile, DFT calculations have been undertaken to investigate the reaction mechanism and chemoselectivity (ring expansion versus spirocyclization). Our mechanistic study indicated that the chemoselectivity is controlled by the competing kinetic and dynamic factors as shown in Figure 1B−D.

■ RESULTS AND DISCUSSION

Experimental Investigations. We commenced our study with 2-propargyl-β-tetrahydrocarboline **1a**, which has a phenyl group at the C1-position, as the standard substrate. To our disappointment, no reaction occurred under our previously reported conditions (1 mol % Ph₃PAuNTf₂, PhMe, 110 °C, 2 h).[14] Then, Brønsted acids, including acetic acid, trifluoroacetic acid, and methanesulfonic acid (MsOH), were considered as additives (see Supporting Information for details). To our delight, when 5 mol % Ph₃PAuNTf₂ and 2.0 equiv of MsOH were used, complete conversion of **1a** was observed after 12 h in dichloromethane (DCM) at room temperature (Table 1, entry

Table 1. Optimization Studies on the Gold-Catalyzed Ring Expansion[a]

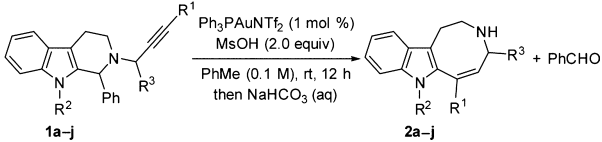| entry	x	y	solvent	time (h)	isolated yield of **2a** (%)
1	5	2.0	DCM	12	72
2	5	2.0	PhMe	2	92
3	5	1.0	PhMe	4	23
4	1	2.0	PhMe	12	90

[a]Reaction conditions: 2-propargyl-β-tetrahydrocarboline **1a**, Ph₃PAuNTf₂ (x mol %), and MsOH (y equiv) in solvent (0.1 M) at room temperature.

1). After basic workup, two products were isolated. The more polar product, **2a**, was confirmed as an azocinoindole containing a secondary amine functionality. The other product with less polarity was identified as benzaldehyde. The yield of **2a** can be improved to 92% when toluene was used as solvent instead of DCM (Table 1, entry 2). When the amount of MsOH was decreased to 1.0 equiv, the conversion dropped dramatically (Table 1, entry 3). However, the ring expansion is not sensitive to the amount of the gold catalyst. When 1 mol % Ph₃PAuNTf₂ was

used, **2a** was obtained in 90% isolated yield (Table 1, entry 4). No reaction occurred in the absence of a gold catalyst.

After obtaining the optimal reaction conditions, we began to investigate the scope of the ring expansion (Table 2). Substrates

### Table 2. Gold-Catalyzed Ring Expansion of 2-Propargyl-β-tetrahydrocarbolines[a]

entry	substrate	R[1]	R[2]	R[3]	2, yield (%)[b]
1	1a	Et	Me	H	2a, 90
2	1b	$^cC_3H_5$	Me	H	2b, 95
3[c]	1c	CH_2OH	Me	H	2c, 61
4	1d	Ph	Me	H	2d, 90
5	1e	$4\text{-}O_2NC_6H_4$	Me	H	2e, 91
6	1f	$4\text{-}MeOC_6H_4$	Me	H	2f, 84
7	1g	$^nC_6H_{13}$	Me	Ph	2g, 66
8	1h	$^nC_6H_{13}$	Me	^{n}Pr	2h, 93
9	1i	$^nC_6H_{13}$	Me	$^cC_3H_5$	2i, 95
10	1j	Et	H	H	2j, 92

[a]Reaction conditions: 2-propargyl-β-tetrahydrocarboline **1**, $Ph_3PAuNTf_2$ (1 mol %), and MsOH (2.0 equiv) in toluene (0.1 M) at room temperature for 12 h unless otherwise specified. [b]Isolated yield. [c]$Ph_3PAuNTf_2$ (5 mol %) and DCM were used.

1a−f bearing terminal alkyl and aryl substituents underwent the ring expansion smoothly, giving azocinoindoles **2a−f** in good to excellent yields (Table 2, entries 1−6). Free hydroxy group can be well tolerated under the reaction conditions (Table 2, entry 3). A variety of alkyl and aryl substituents at the proximal propargylic position are compatible, giving azocinoindoles **2g−i** in yields ranging from 66% to 95% (Table 2, entries 7−9). The absence of the methyl group on the indole nitrogen atom did not interfere with the gold-catalyzed ring expansion, giving azocinoindole **2j** in 92% yield (Table 2, entry 10).

To ascertain whether the phenyl group at the C1-position of β-tetrahydrocarboline is essential, substrates **1k−m** containing alkyl, hydrogen, and ester groups as the C1-substituents were examined (Scheme 2). When substrates **1k** and **1l** were treated

Scheme 2. Gold-Catalyzed Ring Expansion of 2-Propargyl-β-tetrahydrocarbolines 1k−m
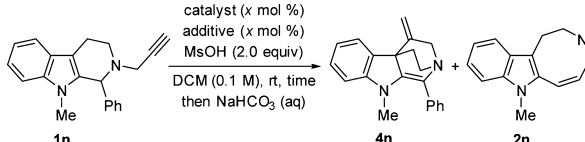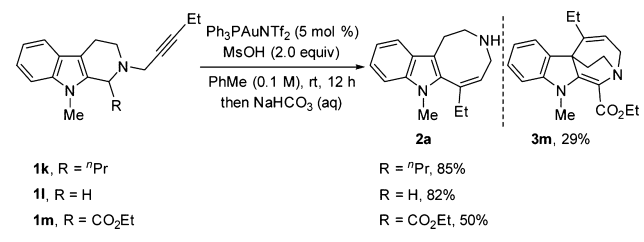

with $Ph_3PAuNTf_2$ and MsOH, the desired ring expansion occurred smoothly to give **2a** in good yields. However, in the case of **1m**, spiroindoline **3m**,[16] together with the ring expansion product **2a**, was isolated. The minor product **3m** was considered to be formed via a gold-catalyzed spirocyclization.

Next, we examined the effects of the terminal substituents. When we treated terminal alkyne substrate **1n** with $Ph_3PAuNTf_2$

and MsOH, we isolated three products, including the spirocyclization product spiroindoline **4n**,[16] the ring expansion product azocinoindole **2n**, and benzaldehyde (Table 3, entry 1). The structure of **4n** was further confirmed by X-ray crystallography (Figure 2).[17]

Table 3. Optimization Studies on the Gold-Catalyzed Spirocyclization[a]

entry	catalyst	additive	x	time (h)	4n/2n[b]	yield of 4n (%)[c]
1	$Ph_3PAuNTf_2$	none	5	2	6:1	80
2	Ph_3PAuCl	AgOTf	5	2	6:1	78
3	Ph_3PAuCl	$AgSbF_6$	5	2	7:1	87
4	IPrAuCl	$AgSbF_6$	5	4	8:1	87
5	JohnPhosAuCl	$AgSbF_6$	5	0.5	>20:1	95
6[d]	$BINAPAu_2Cl_2$	$AgSbF_6$	5	0.5	16:1	90
7	JohnPhosAuCl	$AgSbF_6$	1	0.5	>20:1	95

[a]Reaction conditions: 2-propargyl-β-tetrahydrocarboline **1n**, catalyst (x mol %), additive (x mol %), and MsOH (2.0 equiv) in DCM (0.1 M) at room temperature unless otherwise specified. [b]Determined by ^1H NMR analysis of the crude product. [c]Isolated yield. [d]$BINAPAu_2Cl_2$ (5 mol %) and $AgSbF_6$ (10 mol %) were used. IPr = 1,3-bis(2,6-diisopropylphenyl)imidazol-2-ylidene. JohnPhos = 2-(di-*tert*-butylphosphino)biphenyl. BINAP = (±)-2,2′-bis-(diphenylphosphino)-1,1′-binaphthyl.
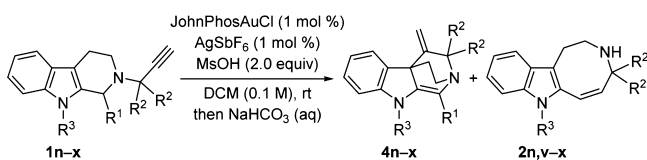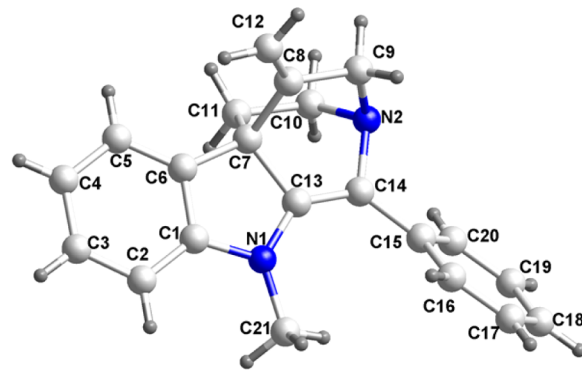

Figure 2. X-ray structure of spiroindoline **4n**.

To improve the chemoselectivity, we tested the effects of both counteranion and ligand (Table 3, entries 2−6). We found that the hexafluoroantimonate anion is slightly preferred over both bis(trifluoromethylsulfonyl)imide and triflate anions in terms of chemoselectivity and the reaction yield. Sterically hindered and electron-rich phosphine ligands, such as JohnPhos and BINAP, gave better results. The combination of JohnPhosAuCl and $AgSbF_6$ displayed the best efficiency, giving the desired spirocyclization product **4n** in 95% isolated yield and the ratio of **4n** to **2n** was enhanced to >20:1 (Table 3, entry 5). Even when the amount of catalyst was reduced from 5 to 1 mol %, the yield did not drop (Table 3, entry 7). Control experiments indicated that both gold catalyst and MsOH are indispensable for the gold-catalyzed spirocyclization (see Supporting Information for details).

The scope of the spirocyclization was further evaluated (Table 4). Terminal alkyne substrates **1n–p** bearing aryl substituents

Table 4. Gold-Catalyzed Spirocyclization of 2-Propargyl-β-tetrahydrocarbolines[a]

| entry	substrate	R[1]	R[2]	R[3]	4/2[b]	4, yield (%)[c]
1	**1n**	Ph	H	Me	>20:1	**4n**, 95
2	**1o**	2-MeOPh	H	Me	15:1	**4o**, 89
3	**1p**	2-O₂NPh	H	Me	4:1	**4p**, 76
4	**1q**	Cy	H	Me	20:1	**4q**, 90
5	**1r**	$^cC_3H_5$	H	Me	>20:1	**4r**, 97
6	**1s**	^nPr	H	Me	>20:1	**4s**, 90
7[d]	**1t**	H	H	Me	>20:1	**4t**, 90
8[d]	**1u**	CO₂Et	H	Me	>20:1	**4u**, 96
9	**1v**	Ph	Me	Me	>20:1	**4v**, 91
10	**1w**	Ph	H	Bn	>20:1	**4w**, 95
11	**1x**	Ph	H	allyl	>20:1	**4x**, 94

[a]Reaction conditions: 2-propargyl-β-tetrahydrocarboline **1**, JohnPhosAuCl (1 mol %), AgSbF₆ (1 mol %), and MsOH (2.0 equiv) in DCM (0.1 M) at room temperature for 0.5 h unless otherwise specified. [b]Determined by ¹H NMR analysis of the crude product. [c]Isolated yield. [d]Reaction time = 12 h.

with different electronic effects at the C1-position of the β-tetrahydrocarboline can undergo the gold(I)-catalyzed spirocyclization smoothly (Table 4, entries 1−3). C1-alkyl substituted substrates **1q−s** performed as well as their aryl substituted counterparts, giving the desired spiroindolines **4q−s** in excellent yields (Table 4, entries 4−6). When the C1-substituent was changed to a hydrogen or an ester group, the rate of the spirocyclization became slower. By extending the reaction time from 0.5 to 12 h, full conversion of the substrates can be achieved and the desired spiroindolines **4t** and **4u** can be generated in 90% and 96% yields, respectively (Table 4, entries 7 and 8). The steric hindrance of the C1- substituent may affect the chemoselectivity. For substrates with bulky 2-MeOPh, 2-O₂NPh and cyclohexyl substituents, the ratio of spiroindoline **4** to azocinoindole **2** decreased to a certain extent (Table 4, entries 2−4). Additionally, substrate **1v**, which contains gem-dimethyl groups at the propargylic position, can also undergo the spirocyclization, giving spiroindoline **4v** in 91% yield (Table 4, entry 9). For substrates containing benzyl and allyl groups on the indole nitrogen atom, the reaction also proceeded very well (Table 4, entries 10 and 11).

Mechanistic Studies. *Proposed Reaction Pathways.* We proposed the following mechanism to account for the reaction outcomes (Scheme 3, the roles of acidic additives are not shown here). The gold-catalyzed reaction starts with the complexation of the alkyne moiety of the substrate to the carbophilic gold catalyst, generating a gold−alkyne complex **A**.[18] Then, the indole moiety undergoes intramolecular nucleophilic attack to the gold-activated triple bond, giving four possible spiroindoline intermediates **B−E**.[19] Among them, **B** and **C** are generated via *endo*-dig cyclizations, whereas **D** and **E** are formed via *exo*-dig cyclizations. Spiroindolines **B** and **D**, which are both α-alkenylation intermediates, may undergo fragmentation to give iminium ions **F** and **H**, respectively. Then, protodeauration[20] and hydrolysis occur to give the ring expansion products (**2** and **5**) and aldehydes. In contrast, β-alkenylation intermediates **C** and **E** can undergo deprotonation at the C1-position by a base to give enamine intermediates **G** and **I**, respectively. Then, the
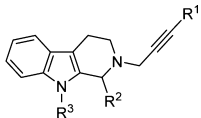
Scheme 3. Proposed Mechanism
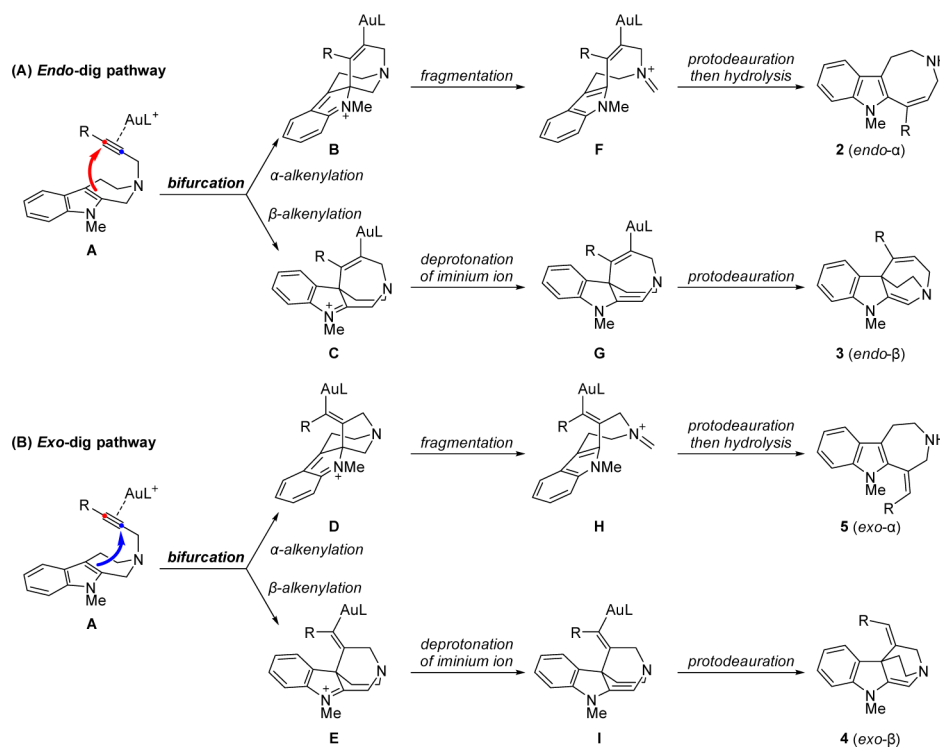
subsequent protodeauration occurs, furnishing the spirocyclization products (**3** and **4**).

DFT calculations have been undertaken (see Computational Methods and Supporting Information for details) to understand the detailed reaction mechanism and how the terminal substituent and the additives used in the reaction system tune the outcome of the gold-catalyzed reaction. Three parts are presented in the following mechanistic study. First, we discussed how intermediates **B**–**E** are formed by using a model reaction of unsubstituted substrate **1y** in the presence of the simplest catalyst $Au(PH_3)^+$ and the simplest acidic additive, proton, in order to achieve detailed information for the initial gold-catalyzed cyclization process (Table 5, entry 1). Then, we used internal

Table 5. Model Systems Studied

entry	1	R^1	R^2	R^3	ligand	acid	solvent
1	**1y**	H	H	H	PH$_3$	H$^+$	DCM
2	**1z**	Me	Me	Me	PMe$_3$	MsOH	PhMe
3	**1aa**	Me	CO$_2$Me	Me	PMe$_3$	MsOH	PhMe
4	**1bb**	H	Me	Me	PMe$_3$	MsOH	DCM

alkyne substrates **1z** and **1aa**, together with terminal alkyne substrate **1bb**, to study how the final products **2**–**5** are generated and to rationalize the regioselectivity (*endo*- versus *exo*-dig pathways) and chemoselectivity (ring expansion versus spirocyclization) (Table 5, entries 2–4). Considering that MsOH is crucial in the reaction system, protonation of the tertiary amine moiety in the substrate by MsOH was taken into account. Finally, we investigated the roles of MsOH in the reaction system.

Surface Bifurcations. We commenced our study by locating *endo*-dig cyclization transition states and intermediates on the PES for **IN3** (Scheme 4). We successfully located the *α*- and *β*-

Scheme 4. Transition States and Intermediates Involved in the *endo*-Dig Cyclization of IN3
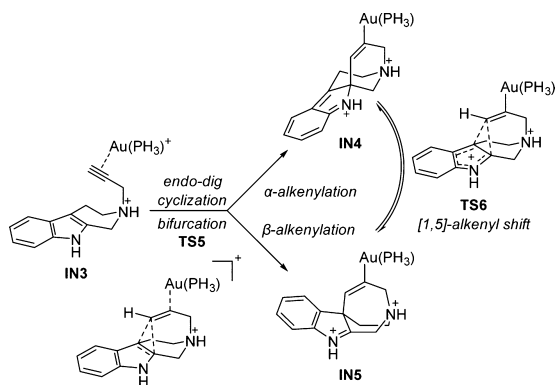
alkenylation intermediates **IN4** and **IN5**, respectively. However, we could only locate one *endo*-dig cyclization transition state **TS5**. To ascertain whether there exists another *endo*-dig cyclization transition state, we performed PES scans by using the distances between the distal C(sp) atom and the carbon atoms at the *α*- and *β*-positions of the indole moiety as variables (Figure 3). DFT calculations indicated that there is indeed only
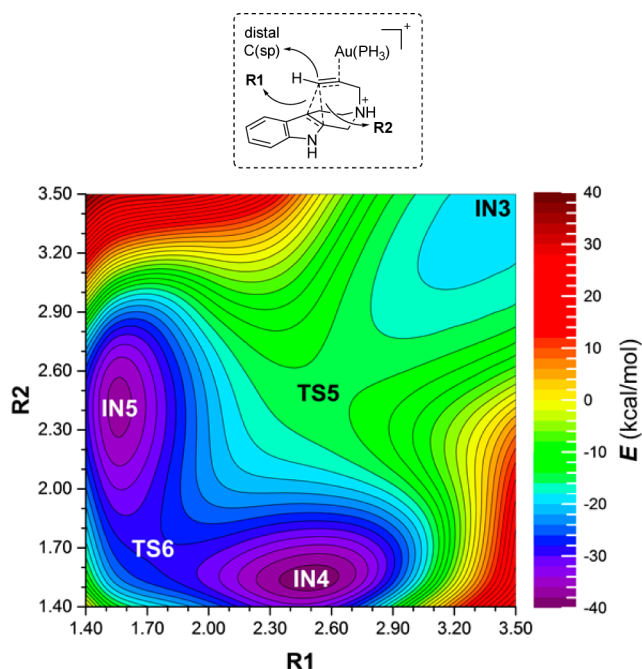

Figure 3. Potential energy surface for the *endo*-dig cyclization of **IN3**. Distances are given in angstroms (Å). See Scheme 4 and Supporting Information for the structures of transition states and intermediates.

one *endo*-dig cyclization transition state on the PES. However, **TS5** leads to two intermediates, **IN4** and **IN5**, simultaneously, which suggests that the PES bifurcates after **TS5**. Moreover, **IN4** and **IN5** are interconvertible via a [1,5]-alkenyl shift transition state **TS6**. Similarly, DFT calculations suggested that surface bifurcation also exists on the PES for *exo*-dig cyclization (see Supporting Information for details).[21]

Rationalization of Regio- and Chemoselectivity. For internal alkyne substrates, only the *endo*-dig cyclization took place (Tables 1 and 2, Scheme 2, *exo*-dig cyclization products **4** and **5** were not observed in all cases). In most cases, the *endo*-dig cyclization only gave the ring expansion product **2** (Tables 1 and 2, Scheme 2). However, for substrate **1m** with an ester group as the C1-substituent, dearomatizing spirocyclization also took place, giving spiroindoline **3m** as a byproduct (Scheme 2).

To understand these results, we performed DFT calculations on the methyl-terminated substrates **1z** and **1aa** with methyl and methoxycarbonyl groups at the C1-position, respectively. There are four possible intramolecular cyclization transition states for each model substrate, depending on the *endo/exo* selectivity and diastereoselectivity induced by the *syn/anti* relationship of the linker and the C1-substituent. DFT calculations suggested that when the C1-methyl group occupies the pseudoequatorial position, the cyclization transition state suffers strong C1-methyl/N9-methyl allylic 1,3-strain (see Supporting Information for details). Therefore, the C1-methyl group prefers to occupy the sterically less hindered pseudoaxial position in all cyclization processes. So we only discussed the favored transition states in this paper.

For substrate **1z**, the *endo*-dig cyclization is favored over the *exo*-dig cyclization by 3.0 kcal/mol (0.4 kcal/mol for **TS7** versus 3.4 kcal/mol for **TS8**, Figure 4, the relative Gibbs free energies for the [1,5]-alkenyl shift transition states in Figures 4, 5, and 7 were set to 0.0 kcal/mol), suggesting that the *endo*-dig cyclization intermediates **IN7** and **IN8** should be generated exclusively. To rationalize this regioselectivity, we performed natural population
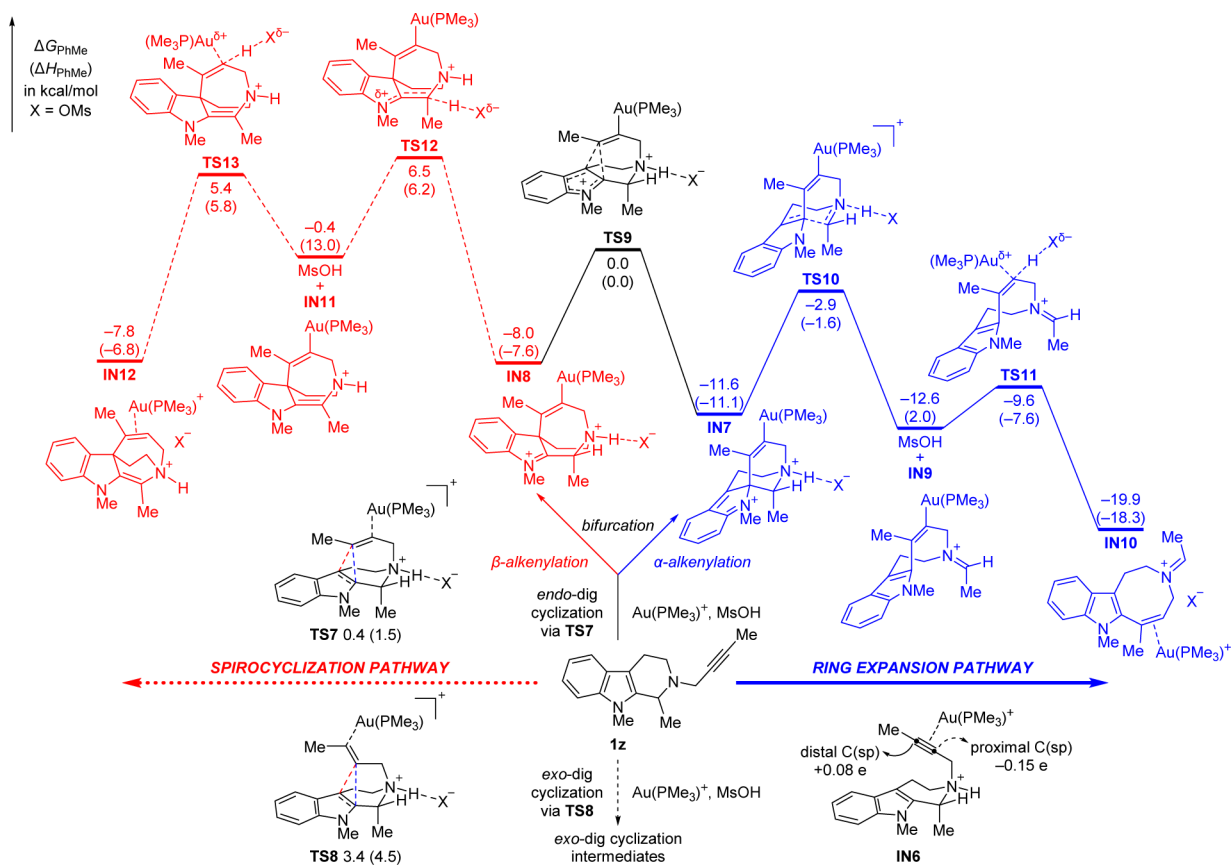
Figure 4. Potential energy surface for substrate **1z** (the reaction is under kinetic control).
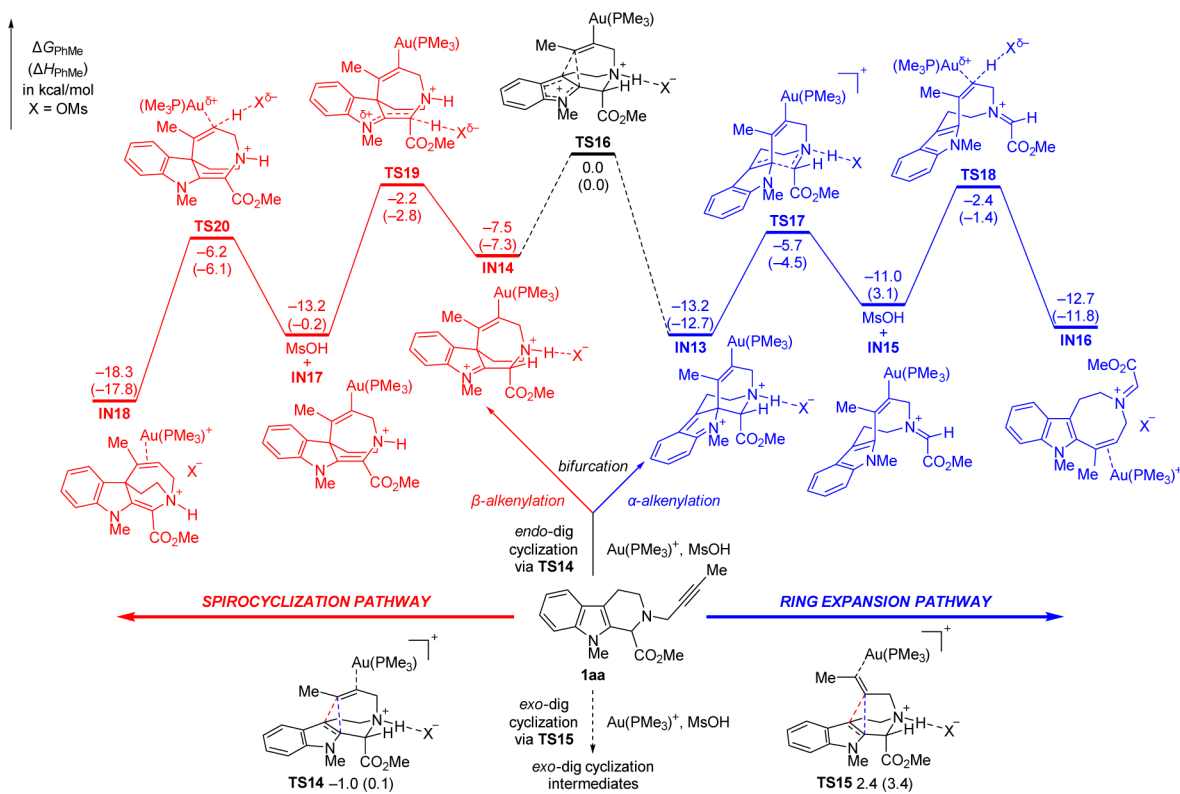

Figure 5. Potential energy surface for substrate **1aa** (the reaction is under dynamic control).

analysis (NPA)[22] on the gold−alkyne complex **IN6** to obtain atomic charges of the distal and proximal carbon atoms on the triple bond.[23] Considering that the terminal methyl group can be regarded as a stronger π-donor than the linker, CH$_2$NR$_2$, owing

to the induction effect induced by the electron-negative nitrogen atom, more positive charge was obtained on the distal C(sp) atom (+0.08 e on the distal C(sp) atom versus −0.15 e on the proximal one, Figure 4, NPA charges). Therefore, the distal C(sp) atom is more electrophilic, and therefore more reactive than the proximal one.

Next, we investigated the chemoselectivity issue. There are three possible reaction pathways for the α-alkenylation intermediate **IN7**. First, **IN7** may be converted back to the starting materials. The second pathway is the [1,5]-alkenyl shift via **TS9**, leading to the β-alkenylation intermediate **IN8**. The third pathway is the ring expansion of **IN7** through a fragmentation/protodeauration mechanism. Considering that the fragmentation of **IN7** via **TS10** (the relative Gibbs free energy for **TS10** is −2.9 kcal/mol) and the subsequent protodeauration of **IN9** via **TS11** (the relative Gibbs free energy for **TS11** is −9.6 kcal/mol) are much faster than the backward reaction to the reactants via **TS7** (the relative Gibbs free energy for **TS7** is 0.4 kcal/mol) and the [1,5]-alkenyl shift via **TS9** (the relative Gibbs free energy for **TS9** is 0.0 kcal/mol), **IN7** should lead to the ring expansion product exclusively.

For the β-alkenylation intermediate **IN8**, the deprotonation by mesylate anion via **TS12** (the relative Gibbs free energy for **TS12** is 6.5 kcal/mol) is disfavored over the endo-dig cyclization via **TS7** (the relative Gibbs free energy for **TS7** is 0.4 kcal/mol) and the [1,5]-alkenyl shift via **TS9** (the relative Gibbs free energy for **TS9** is 0.0 kcal/mol), which indicated that the spirocyclization may not take place. **IN8** should undergo either [1,5]-alkenyl shift via **TS9** or the **IN8** ⇌ **TS7** ⇌ reactants ⇌ **TS7** ⇌ **IN7** + **IN8** pathway, suggesting that although the reaction starts with the surface bifurcation to give both **IN7** and **IN8**, **IN8** can be finally converted to **IN7** exclusively. Consequently, the final product will be the ring expansion product **2** exclusively, which is in good agreement with our experimental observations (Tables 1 and 2, Scheme 2, the spirocyclization product **3** was not formed in most cases).

As depicted in Figure 5, for substrate **1aa**, the shape of the PES changes because the C1-ester group accelerates the deprotonation step in the spirocyclization pathway. In this case, the ring expansion (the rate-limiting transition state in the ring expansion pathway is the protodeauration transition state **TS18** with a relative Gibbs free energy of −2.4 kcal/mol) and the spirocyclization (the rate-limiting transition state in the spirocyclization pathway is a deprotonation transition state **TS19** with a relative Gibbs free energy of −2.2 kcal/mol) are both faster than the [1,5]-alkenyl shift via **TS16** (the relative Gibbs free energy for **TS16** is 0.0 kcal/mol); therefore, **IN13** and **IN14** cannot interconvert through the [1,5]-alkenyl shift in this case.[24] Consequently, both the ring expansion and spirocyclization products can be formed, which is in good accordance with our experiments (Scheme 2). For substrate **1aa**, the distribution of the final products is equal to the ratio of intermediates **IN13** and **IN14**, which is controlled by the shape of the PES. Considering that **IN13** is more stable than **IN14**, the part of bPES leading to **IN13** should be steeper than that leading to **IN14**.[1] Consequently, more ring expansion product should be furnished. Moreover, the difference of the forming C−C bond distances in the cyclization transition state **TS14** also revealed the branching ratio of **IN13** and **IN14**. As shown in Figure 6, the distances between the distal C(sp) and the α/β-carbon of the indole moiety are 2.27 and 2.65 Å, respectively, suggesting that more α-alkenylation intermediate **IN13** should be generated.[2a,b] As a result, more ring expansion product should be formed,
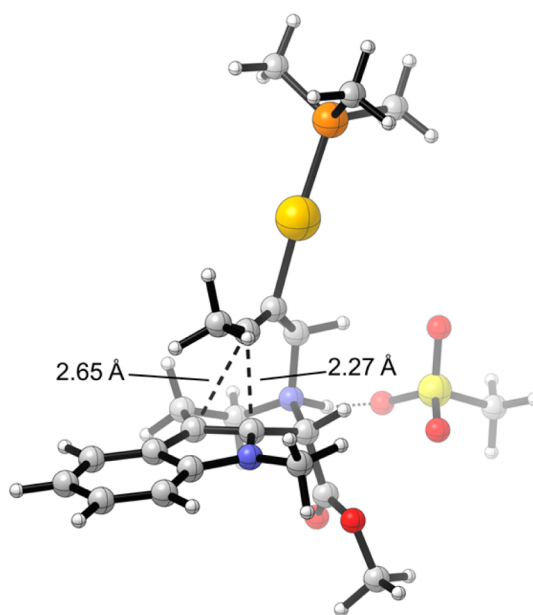

Figure 6. 3D structure for the endo-dig cyclization transition state **TS14**. Color scheme: H, white; C, gray; O, red; P, dark orange; S, yellow; Au, gold.

which is in good agreement with our experimental observations (Scheme 2).

Experimentally, when terminal alkyne was used, both the exo- and endo-products were observed (Tables 3 and 4). The exo-dig cyclization led to the spirocyclization product **4**. No ring expansion product **5** was obtained. In contrast, the endo-dig cyclization gave the ring expansion product **2** exclusively (see minor products in Tables 3 and 4, no spirocyclization product **3** was generated). To understand these experimental results, we performed DFT calculations to obtain both the exo- and endo-PESs for substrate **1bb** (Figure 7).

For terminal alkyne substrate **1bb**, the relative Gibbs free energies for exo- and endo-dig cyclization transition states, **TS21** and **TS22**, respectively, are similar. The exo-dig pathway is slightly favored over the endo-dig pathway by 0.5 kcal/mol (0.6 kcal/mol for **TS21** versus 1.1 kcal/mol for **TS22**, Figure 7A), suggesting that poor exo/endo selectivity in the intramolecular cyclization should be observed when PMe₃ was used as the ligand. Considering that the linker, CH₂NR₂, can be regarded as a stronger π-donor than hydrogen, relatively less negative charge was obtained on the proximal C(sp) atom (−0.06 e on the proximal C(sp) atom versus −0.23 e on the distal one in the gold−alkyne complex **IN19**, Figure 7A, NPA charges).[23] Therefore, the proximal C(sp) atom is more electrophilic than the distal one (although the regioselectivity is poor). Because of the poor exo/endo selectivity of the initial intramolecular cyclization, four cyclization intermediates **IN20−23** should be formed simultaneously (Figure 7).

In the exo-dig pathway, both the α-alkenylation intermediate **IN20** and β-alkenylation intermediate **IN21** can be generated (Figure 7A). We found that **IN20** and **IN21** can interconvert rapidly via a [1,5]-alkenyl shift transition state **TS23** because the relative Gibbs free energy of **TS23** is lower than those of the fragmentation transition state **TS24** in the ring expansion pathway and the deprotonation transition state **TS26** in the spirocyclization pathway (0.0 kcal/mol for **TS23** versus 2.9 kcal/mol for **TS24** and 1.1 kcal/mol for **TS26**). The Curtin−Hammett principle[5] applies, and consequently, the product
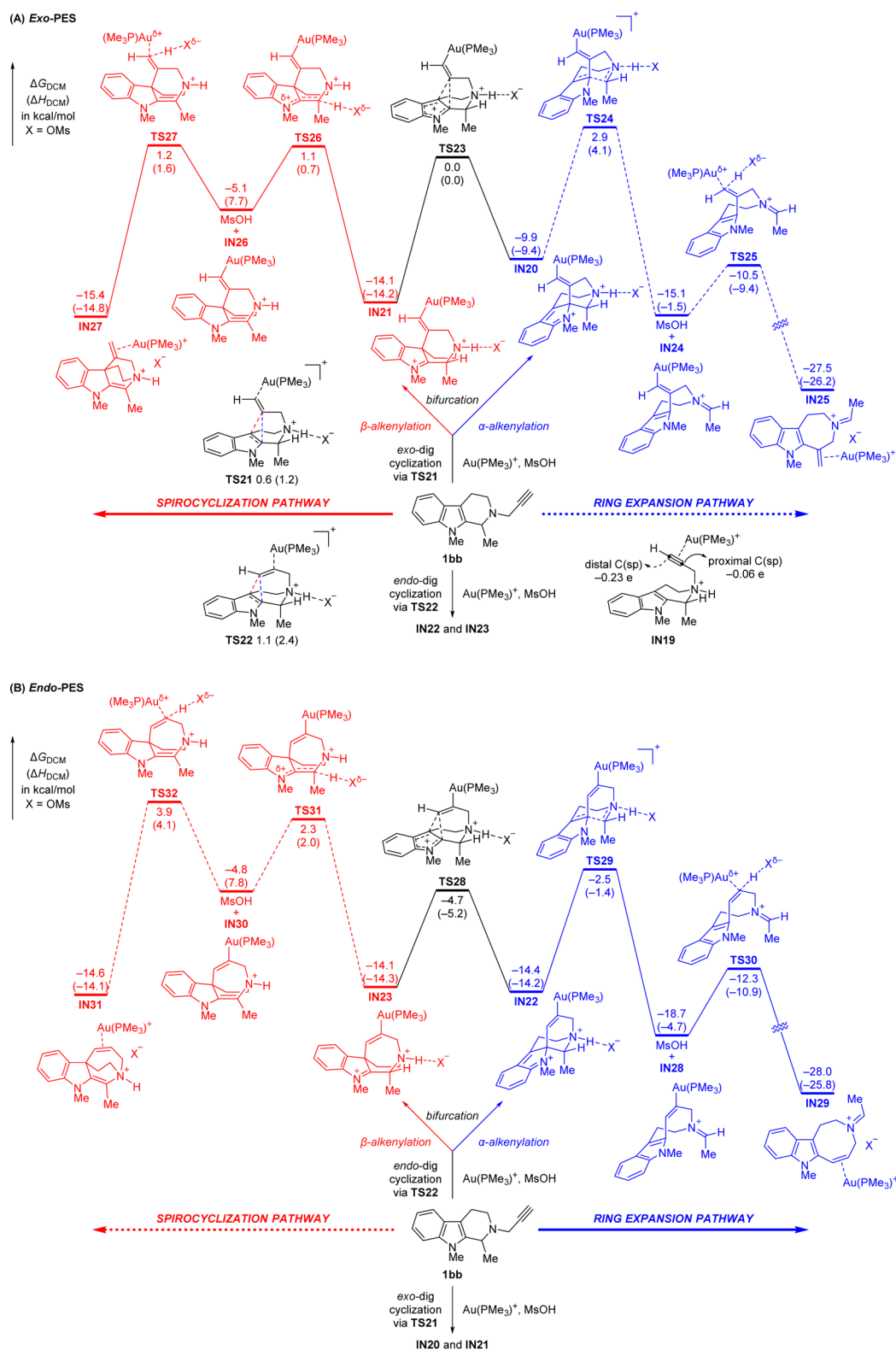
Figure 7. Potential energy surfaces for substrate **1bb** (the reaction is under kinetic control).

distribution is controlled by the relative kinetic preference of the ring expansion and spirocyclization pathways. DFT calculations indicated that the spirocyclization pathway is favored over the ring expansion pathway by 1.7 kcal/mol (1.2 kcal/mol for the rate-limiting protodeauration transition state **TS27** in the spirocyclization pathway versus 2.9 kcal/mol for the rate-limiting fragmentation transition state **TS24** in the ring expansion

pathway). Therefore, the spirocyclization product should be formed predominately, which is in good agreement with our experimental observations (Tables 3 and 4, no ring expansion product **5** was observed in all cases).

In contrast, in the *endo*-dig pathway, the ring expansion pathway is favored over the spirocyclization pathway by 6.4 kcal/mol (Figure 7B, −2.5 kcal/mol for the rate-limiting fragmenta-

Table 6. Activation Gibbs Free Energies for Elementary Steps in the *exo*- and *endo*-Dig Pathways of Substrate 1bb[a]

pathway	ring expansion		spirocyclization	
	fragmentation	protodeauration	deprotonation	protodeauration
exo-dig	12.8	4.6	15.2	6.3
endo-dig	11.9	6.4	16.4	8.7

[a]In kcal/mol.

tion transition state **TS29** in the ring expansion pathway versus 3.9 kcal/mol for the rate-limiting protodeauration transition state **TS32** in the spirocyclization pathway). Therefore, the ring expansion product should be observed exclusively, which is also in good accordance with our experimental results (Tables 3 and 4, no spirocyclization product **3** was observed in all cases).

To rationalize the chemoselectivity, we compared the activation energy of each elementary step in the *exo*- and *endo*-dig pathways (Table 6). We found that the differences are within ca. 1−2 kcal/mol, suggesting that in the *exo*- and *endo*-dig pathways, kinetics of each elementary step do not have significant difference. DFT calculations also indicated that the spirocyclization pathway is intrinsically disfavored over the ring expansion pathway by 2−5 kcal/mol (Table 6). Therefore, when the relative stability of the *α*- and *β*-alkenylation intermediates are similar, the ring expansion pathway should predominate. Indeed, in the *endo*-dig pathway, the *α*-alkenylation intermediate **IN22** has similar stability as that of the *β*-alkenylation intermediate **IN23** (−14.4 kcal/mol for **IN22** versus −14.1 kcal/mol for **IN23**), so the ring expansion product was observed because of the intrinsic preference of the ring expansion.

However, for the *exo*-dig pathway, the shape of the PES changes because the *β*-alkenylation intermediate **IN21** becomes much more stable than the *α*-alkenylation intermediate **IN20** (−14.1 kcal/mol for **IN21** versus −9.9 kcal/mol for **IN20**), in which case, the thermodynamic factor overcomes the intrinsic disadvantage of the spirocyclization pathway and tunes the chemoselectivity toward the spirocyclization pathway. Therefore, the relative thermodynamic stability of the *α*- and *β*-alkenylation intermediates, which is determined by the ring strain in different fused ring systems, controls the relative preference of the spirocyclization and ring expansion pathways; and consequently, determines the product distribution.

As we discussed above, the *exo*-dig cyclization should lead to the spirocyclization product **4**, while the *endo*-dig cyclization is expected to give the ring expansion product **2**. However, if both the *exo*- and *endo*-PESs for substrate **1bb** are taken into consideration, rationalization of the distribution for the final products (the ratio of **4** to **2**) is even more complicated. The rate-limiting step in the *exo*-dig pathway is the protodeauration of **IN26** via **TS27** (the relative Gibbs free energy of **TS27** is 1.2 kcal/mol), while the rate-limiting step in the *endo*-dig pathway is the *endo*-dig cyclization via **TS22** (the relative Gibbs free energy of **TS22** is 1.1 kcal/mol). Considering that the product distribution is determined by the energy difference of **TS27** and **TS22** (−0.1 and 0.8 kcal/mol in terms of Gibbs free energy and enthalpy, respectively), the ratio of **4** to **2** is predicted to be 1:1 to 4:1 when PMe$_3$ was used as the ligand. When the real ligand PPh$_3$ was used, the ratio of **4** to **2** is predicted to be 3:1 to 8:1 (see Supporting Information for details), which is in accordance with the experimental observations (Table 3, entries 1−3, the ratio was 6:1 to 7:1 when PPh$_3$ was used as the ligand). In principle, we may also understand why JohnPhos showed better chemoselectivity than PPh$_3$ (Table 3) by DFT studies if we can locate all the conformations for 12 transition states

involved in Figure 7. However, JohnPhos is large and does not have the C$_3$-axis as PMe$_3$ and PPh$_3$ do, and consequently, hundreds of transition states have to be optimized to give convincing conclusions for the chemoselectivities, which precluded our fully investigations of the reaction system.[25]

Roles of Acidic Additives. The acidic additives have crucial roles in the gold-catalyzed transformations discussed in this paper.[26] The first role is to promote the protodeauration process in the ring expansion pathway (Scheme 3, the F → **2** and H → **5** processes) and maintain the catalytic cycle. The second role is to prevent the formation of unreactive *σ,π*-digold species,[27] which may be generated from terminal alkyne and gold catalyst. Furthermore, DFT calculations indicated that if MsOH is not presented, the activation energy of the fragmentation process in the ring expansion pathway is only ca. 2 kcal/mol; therefore, no spirocyclization product was observed in our previous work.[14] However, if MsOH is added as an additive, the fragmentation process needs a higher activation energy of ca. 8−13 kcal/mol, making the spirocyclization pathway compete with the ring expansion pathway. In this case, the chemoselectivity (ring expansion versus spirocyclization) can be tuned by the substituent effect and reaction conditions. We reasoned that the hyperconjugation interaction between the nonbonding orbital of the N(sp^3) atom and the C−C antibonding orbital, which stabilizes the fragmentation transition state, was reduced if the tertiary amine moiety was protonated (Scheme 5).

Scheme 5. Hyperconjugation Interaction between the Nonbonding Orbital of the N(sp^3) Atom and the C−C Antibonding Orbital in B and D
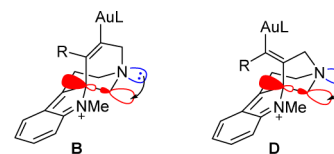
CONCLUSIONS

We have disclosed two transformations of 2-propargyl-*β*-tetrahydrocarbolines under gold catalysis in the presence of methanesulfonic acid. When internal alkyne substrate was used, ring expansion took place, giving the azocinoindole derivative, which is the skeleton of many natural alkaloids, in excellent yields (Tables 1 and 2, Scheme 2). In contrast, when terminal alkyne was used as the substrate, dearomatizing spirocyclization occurred to furnish the spiroindoline product predominantly (Tables 3 and 4). DFT calculations indicated that the initial intramolecular cyclization of the gold-activated 2-propargyl-*β*-tetrahydrocarboline contains a bifurcating potential energy surface, giving *α*- and *β*-alkenylation intermediates simultaneously. The *exo/endo* selectivity of the intramolecular cyclization can be tuned by the electronic effect of the terminal substituent on the alkyne moiety. Then, the *exo*- or *endo*-dig cyclization intermediates may undergo either the ring expansion

(through fragmentation/protodeauration mechanism) or spirocyclization (through deprotonation/protodeauration mechanism) pathways. The α- and β-alkenylation intermediates can interconvert into each other via a [1,5]-alkenyl shift transition state. The reaction selectivity is controlled by the relative energies of the intramolecular cyclization, [1,5]-alkenyl shift, ring expansion, and spirocyclization processes. If the interconversion of the α- and β-alkenylation intermediates is faster than the ring expansion and spirocyclization processes, the chemoselectivity is determined by the relative preference of the ring expansion versus spirocyclization pathways. In this case, the reaction is under typical kinetic control (Figures 4 and 7). In contrast, if the [1,5]-alkenyl shift is slower than both the ring expansion and spirocyclization processes, the product distribution is determined by dynamic factors (Figure 5). To the best of our knowledge, this work represents the first observations of all three situations depicted in Figure 1B−D in one reaction system, shedding some light on the determinants for selectivity on a bifurcating potential energy surface. Further applications of the ring expansion are underway in our lab.

■ COMPUTATIONAL METHODS

All DFT calculations were performed with the Gaussian 09 software package.[28] Solution-phase relaxed PES scans and geometry optimizations of all the minima and transition states involved were carried out using the B3LYP functional[29] and IEFPCM calculation with radii and nonelectrostatic terms for SMD solvation model.[30] PhMe was used as solvent for internal alkyne substrates, while DCM was used for terminal ones. The SDD basis set[31] (Stuttgart/Dresden ECP) was used for gold and the 6-31G(d) basis set[32] for the other atoms. We labeled this basis set as SDD-6-31G(d). The keyword "5D" was used to specify that five d-type orbitals were used for all elements in the calculations. Frequency calculations at the same level were performed to validate each structure as either a minimum or a transition state and to evaluate its zero-point energy and thermal corrections at 298 K. Quasiharmonic corrections were applied during the entropy calculations by setting all positive frequencies that are less than $100 \ cm^{-1}$ to $100 \ cm^{-1}$.[33] A standard state of 298 K and 1 mol/L was used for calculating thermal corrections. Solution-phase single point energy calculations (SDD basis set[31] (Stuttgart/Dresden ECP) was used for gold and the 6-311+G(d,p) basis set[32] for the other atoms) were performed using the B3LYP functional with the D3 version of Grimme's dispersion[34] (with Becke-Johnson damping) based on the optimized structures from the SMD/B3LYP/SDD-6-31G(d) method. All discussed energies were Gibbs free energies unless otherwise specified. Enthalpies were also given for reference. Assessment of other density functionals can be found in Supporting Information. 3D structure for **TS14** was prepared with CYLview.[35]

■ ASSOCIATED CONTENT

ⓢ Supporting Information

The Supporting Information is available free of charge on the ACS Publications website at DOI: 10.1021/jacs.5b05971.

> Experimental procedures, characterization data, copies of ^{1}H and ^{13}C NMR spectra, and computational details (PDF)
> Crystallographic data for **4n** (CIF)

■ AUTHOR INFORMATION

Corresponding Authors
*yuzx@pku.edu.cn
*wangsz@nju.edu.cn

Author Contributions
§L.Z. and Y.W. contributed equally.

■ REFERENCES

(1) For reviews, see: (a) Ess, D. H.; Wheeler, S. E.; Iafe, R. G.; Xu, L.; Çelebi-Ölçüm, N.; Houk, K. N. *Angew. Chem., Int. Ed.* **2008**, *47*, 7592. (b) Rehbein, J.; Carpenter, B. K. *Phys. Chem. Chem. Phys.* **2011**, *13*, 20906.

(2) For selected examples, see: (a) Çelebi-Ölçüm, N.; Ess, D. H.; Aviyente, V.; Houk, K. N. *J. Am. Chem. Soc.* **2007**, *129*, 4528. (b) Çelebi-Ölçüm, N.; Ess, D. H.; Aviyente, V.; Houk, K. N. *J. Org. Chem.* **2008**, *73*, 7472. (c) Thomas, J. B.; Waas, J. R.; Harmata, M.; Singleton, D. A. *J. Am. Chem. Soc.* **2008**, *130*, 14544. (d) Hong, Y. J.; Tantillo, D. J. *Nat. Chem.* **2009**, *1*, 384. (e) Hansen, J. H.; Gregg, T. M.; Ovalles, S. R.; Lian, Y.; Autschbach, J.; Davies, H. M. L. *J. Am. Chem. Soc.* **2011**, *133*, 5076. (f) Siebert, M. R.; Zhang, J.; Addepalli, S. V.; Tantillo, D. J.; Hase, W. L. *J. Am. Chem. Soc.* **2011**, *133*, 8335. (g) Hong, Y. J.; Tantillo, D. J. *Nat. Chem.* **2014**, *6*, 104. (h) Pham, H. V.; Houk, K. N. *J. Org. Chem.* **2014**, *79*, 8968.

(3) For reports on gold-catalyzed transformations involving bifurcating potential energy surfaces, see: (a) Garayalde, D.; Gómez-Bengoa, E.; Huang, X.; Goeke, A.; Nevado, C. *J. Am. Chem. Soc.* **2010**, *132*, 4720. (b) Wang, Z. J.; Benitez, D.; Tkatchouk, E.; Goddard, W. A., III; Toste, F. D. *J. Am. Chem. Soc.* **2010**, *132*, 13064. (c) Noey, E. L.; Wang, X.; Houk, K. N. *J. Org. Chem.* **2011**, *76*, 3477. (d) Ye, L.; Wang, Y.; Aue, D. H.; Zhang, L. *J. Am. Chem. Soc.* **2012**, *134*, 31. (e) Hansmann, M. M.; Rudolph, M.; Rominger, F.; Hashmi, A. S. K. *Angew. Chem., Int. Ed.* **2013**, *52*, 2593. (f) Wang, Y.; Yepremyan, A.; Ghorai, S.; Todd, R.; Aue, D. H.; Zhang, L. *Angew. Chem., Int. Ed.* **2013**, *52*, 7795. (g) Vilhelmsen, M. H.; Hashmi, A. S. K. *Chem. - Eur. J.* **2014**, *20*, 1901. (h) Hansmann, M. M.; Tšupova, S.; Rudolph, M.; Rominger, F.; Hashmi, A. S. K. *Chem. - Eur. J.* **2014**, *20*, 2215. (i) Vummaleti, S. V. C.; Falivene, L.; Poater, A.; Cavallo, L. *ACS Catal.* **2014**, *4*, 1287. (j) Tudela, E.; González, J.; Vicente, R.; Santamaría, J.; Rodríguez, M. A.; Ballesteros, A. *Angew. Chem., Int. Ed.* **2014**, *53*, 12097.

(4) In general, whether the bifurcation process is reversible or not does not influence the discussion of determinants for product distribution shown in Figure 1B−D. Moreover, we hypothesized that nonstatistical dynamic effects were important only for **TS1** which leads to surface bifurcation. The discussions on the other transition states were based on classical transition state theory in which dynamic effects are not present.

(5) For one review, see: Seeman, J. I. *Chem. Rev.* **1983**, *83*, 83.

(6) For selected reviews on gold catalysis, see: (a) Hashmi, A. S. K.; Hutchings, G. J. *Angew. Chem., Int. Ed.* **2006**, *45*, 7896. (b) Jiménez-Núñez, E.; Echavarren, A. M. *Chem. Commun.* **2007**, *43*, 333. (c) Fürstner, A.; Davies, P. W. *Angew. Chem., Int. Ed.* **2007**, *46*, 3410. (d) Hashmi, A. S. K.; Rudolph, M. *Chem. Soc. Rev.* **2008**, *37*, 1766. (e) Li, Z.; Brouwer, C.; He, C. *Chem. Rev.* **2008**, *108*, 3239. (f) Gorin, D. J.; Sherry, B. D.; Toste, F. D. *Chem. Rev.* **2008**, *108*, 3351. (g) Fürstner, A. *Chem. Soc. Rev.* **2009**, *38*, 3208. (h) Hashmi, A. S. K. *Angew. Chem., Int. Ed.* **2010**, *49*, 5232. (i) Rudolph, M.; Hashmi, A. S. K. *Chem. Soc. Rev.* **2012**, *41*, 2448. (j) Hashmi, A. S. K. *Acc. Chem. Res.* **2014**, *47*, 864. (k) Wang, Y.-M.; Lackner, A. D.; Toste, F. D. *Acc. Chem. Res.* **2014**, *47*, 889.

(7) For selected reports on the construction of azocinoindoles, see: (a) Yoneda, R.; Kimura, T.; Kinomoto, J.; Harusawa, S.; Kurihara, T. *J. Heterocycl. Chem.* **1996**, *33*, 1909. (b) Baran, P. S.; Corey, E. J. *J. Am. Chem. Soc.* **2002**, *124*, 7904. (c) Baran, P. S.; Guerrero, C. A.; Corey, E. J. *J. Am. Chem. Soc.* **2003**, *125*, 5628. (d) Voskressensky, L. G.; Borisova, T.

N.; Kulikova, L. N.; Varlamov, A. V.; Catto, M.; Altomare, C.; Carotti, A. *Eur. J. Org. Chem.* **2004**, *2004*, 3128. (e) Arai, S.; Nakajima, M.; Nishida, A. *Angew. Chem., Int. Ed.* **2014**, *53*, 5569. (f) Jin, S.; Gong, J.; Qin, Y. *Angew. Chem., Int. Ed.* **2015**, *54*, 2228.

(8) For azocinoindole synthesis via gold catalysis, see: (a) Ferrer, C.; Echavarren, A. M. *Angew. Chem., Int. Ed.* **2006**, *45*, 1105. (b) Ferrer, C.; Amijs, C. H. M.; Echavarren, A. M. *Chem. - Eur. J.* **2007**, *13*, 1358. (c) Ferrer, C.; Escribano-Cuesta, A.; Echavarren, A. M. *Tetrahedron* **2009**, *65*, 9015. (d) Modha, S. G.; Vachhani, D. D.; Jacobs, J.; Meervelt, L. V.; Van der Eycken, E. V. *Chem. Commun.* **2012**, *48*, 6550. (e) Peshkov, V. A.; Pereshivko, O. P.; Van der Eycken, E. V. *Adv. Synth. Catal.* **2012**, *354*, 2841. (f) Vachhani, D. D.; Kumar, A.; Modha, S. G.; Sharma, S. K.; Parmar, V. S.; Van der Eycken, E. V. *Synthesis* **2015**, *47*, 1337.

(9) (a) Murao, S.; Hayashi, H.; Takiuchi, K.; Arai, M. *Agric. Biol. Chem.* **1988**, *52*, 885. (b) Hayashi, H.; Takiuchi, K.; Murao, S.; Arai, M. *Agric. Biol. Chem.* **1988**, *52*, 2131. (c) Hayashi, H.; Takiuchi, K.; Murao, S.; Arai, M. *Agric. Biol. Chem.* **1989**, *53*, 461. (d) Hayashi, H.; Asabu, Y.; Murao, S.; Arai, M. *Biosci., Biotechnol., Biochem.* **1995**, *59*, 246. (e) Hayashi, H.; Furutsuka, K.; Shiono, Y. *J. Nat. Prod.* **1999**, *62*, 315. (f) Shiono, Y.; Akiyama, K.; Hayashi, H. *Biosci., Biotechnol., Biochem.* **1999**, *63*, 1910. (g) Shiono, Y.; Akiyama, K.; Hayashi, H. *Biosci., Biotechnol., Biochem.* **2000**, *64*, 103.

(10) Yap, W.-S.; Gan, C.-Y.; Low, Y.-Y.; Choo, Y.-M.; Etoh, T.; Hayashi, M.; Komiyama, K.; Kam, T.-S. *J. Nat. Prod.* **2011**, *74*, 1309.

(11) (a) Kam, T.-S.; Yoganathan, K.; Chuah, C.-H. *Tetrahedron Lett.* **1995**, *36*, 759. (b) Kam, T.-S.; Lim, K.-H.; Yoganathan, K.; Hayashi, M.; Komiyama, K. *Tetrahedron* **2004**, *60*, 10739.

(12) (a) Awang, K.; Sévenet, T.; Hadi, A. H. A.; David, B.; Païs, M. *Tetrahedron Lett.* **1992**, *33*, 2493. (b) Awang, K.; Sévenet, T.; Païs, M.; Hadi, A. H. A. *J. Nat. Prod.* **1993**, *56*, 1134.

(13) For selected reviews on the synthesis of medium-sized heterocycles, see: (a) Yet, L. *Chem. Rev.* **2000**, *100*, 2963. (b) Majumdar, K. C. *RSC Adv.* **2011**, *1*, 1152. (c) Sharma, A.; Appukkuttan, P.; Van der Eycken, E. *Chem. Commun.* **2012**, *48*, 1623. (d) Kaur, N.; Kishore, D. *Synth. Commun.* **2014**, *44*, 2577.

(14) Zhang, L.; Chang, L.; Hu, H.; Wang, H.; Yao, Z.-J.; Wang, S. *Chem. - Eur. J.* **2014**, *20*, 2925.

(15) For selected reviews on dearomatization of heterocycles, see: (a) Roche, S. P.; Porco, J. A., Jr. *Angew. Chem., Int. Ed.* **2011**, *50*, 4068. (b) Zhuo, C.-X.; Zhang, W.; You, S.-L. *Angew. Chem., Int. Ed.* **2012**, *51*, 12662. (c) Ding, Q.; Zhou, X.; Fan, R. *Org. Biomol. Chem.* **2014**, *12*, 4807.

(16) The structures of spiroindolines **3** and **4** are related to those of twisted amides containing nitrogen at the bridgehead position. For selected reviews on twisted amides, see: (a) Hall, H. K., Jr.; El-Shekeil, A. *Chem. Rev.* **1983**, *83*, 549. (b) Szostak, M.; Aubé, J. *Chem. Rev.* **2013**, *113*, 5701.

(17) CCDC 1005625 (**4n**) contains the supplementary crystallographic data for this paper. These data can be obtained free of charge from The Cambridge Crystallographic Data Centre via www.ccdc.cam.ac.uk/data_request/cif.

(18) Pernpointner, M.; Hashmi, A. S. K. *J. Chem. Theory Comput.* **2009**, *5*, 2717.

(19) For selected reports on the transformation of spirocyclic intermediates in gold catalysis, see: (a) Hashmi, A. S. K.; Yang, W.; Rominger, F. *Adv. Synth. Catal.* **2012**, *354*, 1273. (b) Hashmi, A. S. K.; Yang, W.; Rominger, F. *Chem. - Eur. J.* **2012**, *18*, 6576. (c) Hashmi, A. S. K.; Häffner, T.; Yang, W.; Pankajakshan, S.; Schäfer, S.; Schultes, L.; Rominger, F.; Frey, W. *Chem. - Eur. J.* **2012**, *18*, 10480.

(20) (a) Krauter, C. M.; Hashmi, A. S. K.; Pernpointer, M. *ChemCatChem* **2010**, *2*, 1226. (b) Biasiolo, L.; Trinchillo, M.; Belanzoni, P.; Belpassi, L.; Busico, V.; Ciancaleoni, G.; D'Amora, A.; Macchioni, A.; Tarantelli, F.; Zuccaccia, D. *Chem.- Eur. J.* **2014**, *20*, 14594. (c) BabaAhmadi, R.; Ghanbari, P.; Rajabi, N. A.; Hashmi, A. S. K.; Yates, B. F.; Ariafard, A. *Organometallics* **2015**, *34*, 3186.

(21) If the nitrogen atom was not protonated, the surface bifurcation still took place, suggesting that surface bifurcations are also involved in our previous work (ref 14). See Supporting Information for details.

(22) *NBO* Version 3.1, Glendening, E. D.; Reed, A. E.; Carpenter, J. E.; Weinhold, F.

(23) (a) Gilmore, K.; Alabugin, I. V. *Chem. Rev.* **2011**, *111*, 6513. (b) Hashmi, A. S. K.; Schuster, A. M.; Gaillard, S.; Cavallo, L.; Poater, A.; Nolan, S. P. *Organometallics* **2011**, *30*, 6328. (c) Dong, Z.; Liu, C.-H.; Wang, Y.; Lin, M.; Yu, Z.-X. *Angew. Chem., Int. Ed.* **2013**, *52*, 14157.

(24) The relative energy of the *exo*-dig cyclization transition state **TS15** is higher than that of the [1,5]-alkenyl shift transition state **TS16** by 2.4 kcal/mol, which is in accordance with the experimental observations that no *exo*-cyclization products were observed.

(25) Our preliminary DFT studies showed that searching only limited numbers of transition states cannot provide convincing conclusions. See Supporting Information for details.

(26) Another potential role of the acid is to increase the induction effect of the nitrogen atom in the regioselectivity-determining step. Although it is correct theoretically, whether the nitrogen atom was protonated did not influence the energy difference of the *exo*- and *endo*-dig cyclizations significantly. See Supporting Information for details.

(27) Grirrane, A.; Garcia, H.; Corma, A.; Álvarez, E. *ACS Catal.* **2011**, *1*, 1647.

(28) *Gaussian 09*, Revision D.01, Frisch, M. J.; Trucks, G. W.; Schlegel, H. B.; Scuseria, G. E.; Robb, M. A.; Cheeseman, J. R.; Scalmani, G.; Barone, V.; Mennucci, B.; Petersson, G. A.; Nakatsuji, H.; Caricato, M.; Li, X.; Hratchian, H. P.; Izmaylov, A. F.; Bloino, J.; Zheng, G.; Sonnenberg, J. L.; Hada, M.; Ehara, M.; Toyota, K.; Fukuda, R.; Hasegawa, J.; Ishida, M.; Nakajima, T.; Honda, Y.; Kitao, O.; Nakai, H.; Vreven, T.; Montgomery, J. A., Jr.; Peralta, J. E.; Ogliaro, F.; Bearpark, M.; Heyd, J. J.; Brothers, E.; Kudin, K. N.; Staroverov, V. N.; Kobayashi, R.; Normand, J.; Raghavachari, K.; Rendell, A.; Burant, J. C.; Iyengar, S. S.; Tomasi, J.; Cossi, M.; Rega, N.; Millam, J. M.; Klene, M.; Knox, J. E.; Cross, J. B.; Bakken, V.; Adamo, C.; Jaramillo, J.; Gomperts, R.; Stratmann, R. E.; Yazyev, O.; Austin, A. J.; Cammi, R.; Pomelli, C.; Ochterski, J. W.; Martin, R. L.; Morokuma, K.; Zakrzewski, V. G.; Voth, G. A.; Salvador, P.; Dannenberg, J. J.; Dapprich, S.; Daniels, A. D.; Farkas, Ö.; Foresman, J. B.; Ortiz, J. V.; Cioslowski, J.; Fox, D. J.; Gaussian, Inc.: Wallingford, CT, 2013.

(29) (a) Becke, A. D. *J. Chem. Phys.* **1993**, *98*, 5648. (b) Lee, C.; Yang, W.; Parr, R. G. *Phys. Rev. B: Condens. Matter Mater. Phys.* **1988**, *37*, 785.

(30) Marenich, A. V.; Cramer, C. J.; Truhlar, D. G. *J. Phys. Chem. B* **2009**, *113*, 6378.

(31) Andrae, D.; Häußermann, U.; Dolg, M.; Stoll, H.; Preuß, H. *Theor. Chim. Acta* **1990**, *77*, 123.

(32) Hehre, W. J.; Radom, L.; Schleyer, P. v. R.; Pople, J. A. *Ab Initio Molecular Orbital Theory*; Wiley: New York, 1986.

(33) (a) Zhao, Y.; Truhlar, D. G. *Phys. Chem. Chem. Phys.* **2008**, *10*, 2813. (b) Ribeiro, R. F.; Marenich, A. V.; Cramer, C. J.; Truhlar, D. G. *J. Phys. Chem. B* **2011**, *115*, 14556.

(34) (a) Grimme, S.; Antony, J.; Ehrlich, S.; Krieg, H. *J. Chem. Phys.* **2010**, *132*, 154104. (b) Grimme, S.; Ehrlich, S.; Goerigk, L. *J. Comput. Chem.* **2011**, *32*, 1456.

(35) Legault, C. Y. *CYLview*, 1.0b; Université de Sherbrooke, 2009. http://www.cylview.org.